



Hydraulic Optimization and Experimental Measurement of Low Specific Speed Centrifugal Fire Pump

J. B. Hu¹, R. Y. Xue¹, H. L. Liu¹, K. Wang^{1,2†} and X. Lu³

¹ Research Center of Fluid Machinery Engineering and Technology, Jiangsu University, Zhenjiang, Jiangsu Province, 212013, China

² Xinxiang Aviation Industry (Group) Co., Ltd., Xinxiang, Henan Province, 453003, China

³ Xi'an Aerospace Propulsion Institute, Xi'an, Shanxi Province, 710199, China

†Corresponding Author Email: wangkai@ujs.edu.cn

(Received April 4, 2022; accepted May 21, 2022)

ABSTRACT

As one of the core components of the fire-fighting water-supply system, the performance of a fire pump directly determines the extent of damage caused by the fire. Compared with conventional pumps, the design requirements of fire pumps not only need to ensure that the head of the pump is at $0Q_d$, $1.0Q_d$, and $1.5Q_d$ and its efficiency is at $1.0Q_d$ but also consider the cavitation performance at each flow rate, which presents a greater challenge for the design of high-performance fire pumps. By optimizing the design of a centrifugal fire pump with a specific speed of 24.7, numerical calculations were performed to obtain the best optimized scheme Y4. The results show that at the design flow rate the best optimized scheme improves the efficiency by 9.17% compared with the original scheme, and the head meets the design requirements of the fire pump while avoiding the hump phenomenon. Through a comparative analysis, it was found that the optimized scheme Y4 can reduce the pressure pulsations at the outlet of the pump and improve the cavitation performance at each flow rate. The experiment verifies that the head of the best optimized scheme at the design flow rate is 74.43m, the pump efficiency is 40.22%, and there is no hump in the head curve, which can meet the design and use requirements of the fire pump. The maximum reduction in the outlet pressure pulsations coefficient in the best optimized scheme was 47.12% on average. Compared with the original scheme, the critical net positive suction head ($NPSH_r$) of the best optimized scheme was reduced by 21.5%, 17.6%, 15.7%, and 16.8%, respectively.

Keywords: Low specific speed centrifugal pump; Efficiency; Hump; Pressure pulsations; NPSH.

NOMENCLATURE

b_2	blade outlet width	P_{in}	absolute pressure at the pump inlet
C_p	pressure pulsations coefficient	P_v	vapor pressure of the water
H	head	Q_d	design flow rate
H_d	head at a design flow rate	u	circumferential speed of the impeller outlet
$NPSH$	Net Positive Suction Head	v_{in}	absolute velocity at the pump inlet
$NPSH_r$	Critical Net Positive Suction Head	β_2	blade outlet angle
P	static pressure	η	efficiency
\bar{P}	average of the static pressure	ρ	density of the water

1. INTRODUCTION

Fire has been a universal disaster faced by the world for a long time and is one of the most frequent disasters in the world. Smoke and toxic gases produced by fires can directly or indirectly affect the environment. While people are concerned about casualties and property damage, the environmental

pollution caused by fires is often overlooked. In recent years, as people have become more aware of environmental protection, quickly and successfully extinguishing fires and protecting the surrounding environment from fire damage has become a topic that firefighters cannot ignore. Fire pumps are one of the most important core components of fire-fighting water supply systems, and their reliability directly determines the extent of fire spread and damage.

There are many forms of fire-fighting equipment and [Menin and Iguama \(2006\)](#) found that hydraulically driven fire pumps are less expensive to maintain than diesel-driven pumps and can cope with extreme conditions. With the development of fire-fighting systems, centrifugal pumps are increasingly being used in fire-fighting. To obtain the optimum mass dimensional parameters for centrifugal fire pumps, [Vasiljeva *et al.* \(2020\)](#) developed an optimized mathematical model that enables centrifugal pumps for fire-fighting to be designed in such a way that the weight of the pump is minimized while ensuring high reliability. To attain centrifugal fire pumps with excellent performance, splitter blades ([Shi *et al.* 2009](#); [Yuan and Yuan 2017](#); [Rosa Emerick 2020](#); [Namazizadeh *et al.* 2020](#); [Chabannes *et al.* 2021](#); [Adu *et al.* 2021](#)) were used to change the internal flow characteristics of low-specific-speed centrifugal fire pumps, and [Yang *et al.* \(2017\)](#) used an increased flow rate design method. [Zhang *et al.* \(2020\)](#) used NSGA-II and RBF hybrid algorithms to optimize the efficiency and head of the centrifugal pump, and [Xu *et al.* \(2016\)](#) used the orthogonal optimization method to select parameters, such as blade wrap angle, blade inlet, and outlet angle of a centrifugal pump to optimize the efficiency and cavitation performance of the centrifugal pump. To improve the efficiency of centrifugal pumps, [Kocaaslan *et al.* \(2016\)](#) optimized geometric parameters, such as the impeller inlet and outlet diameters, blade inlet and outlet angles, blade wrap angle, blade thickness, blade inlet, and outlet width. [Zhang *et al.* \(2021\)](#) used particle swarm optimization algorithms to optimize the design of a vertical long-shaft fire pump to achieve an overload-free design. [Paluch and Noga \(2020\)](#) proposed a single-stage centrifugal pump impeller design for fire engines.

According to “Standard for the Installation of Stationary Pumps for Fire Protection (NFPA 20-2019),” the design of fire pumps must follow the following regulations: (1) The curve of flow rate is flat and smooth without the hump; (2) The actual head of the fire pump at $0Q_d$ shall not be greater than 1.4 times of the design flow rate; (3) The actual head at $1.5Q_d$ is not less than 0.65 times of the design flow rate. Therefore, the design of centrifugal fire pumps needs to consider the heads of $0Q_d$, $1.0Q_d$, and $1.5Q_d$ at the same time simultaneously and consider the efficiency and cavitation, which puts forward high requirements for the hydraulic design of the centrifugal fire pump. At present, there is little research on the performance of centrifugal fire pump design regulations, and even less development of centrifugal fire pump design methods and high-performance hydraulic models to meet the design requirements of fire pumps. Therefore, the design of a centrifugal fire pump with high efficiency, good cavitation performance, and flat head curve is not only of high theoretical and practical value but also has high social benefits for the development of the fire-fighting industry and the safety of people and property; therefore, the research has great potential and important significance.

A hydraulic model of the fire pump with excellent performance consists of a fire pump model using a

low-specific-speed centrifugal pump and a hydraulic design of centrifugal fire pump, which combines numerical calculations and experiments. It provides technical support for the design of the centrifugal fire pumps and enriches the high-performance hydraulic model of fire pumps.

2. EXPERIMENTAL MEASUREMENT

2.1 Research Model

The research object was a 6-blade centrifugal fire pump with a specific speed n_s ($n_s = 3.65n_d \sqrt{Q_d} / H_d^{0.75}$ where, n_d , Q_d , and H_d are rpm, m^3/s , and m respectively) of 24.7; the main design parameters are as follows: The design flow rate Q_d was $12.5m^3/h$, head H_d was 74 m, and efficiency η is equal to or greater than 38%. The fire pump includes an impeller, volute, pump shaft, pump chambers, and other components. A schematic of the fire pump structure is shown in Fig. 1, and the physical object of the fire pump is shown in Fig. 2. The inlet diameter of the impeller was 68mm, outlet diameter of the impeller was 228mm, outlet width of the impeller was 7 mm, and throat area of the volute was $1025 mm^2$.

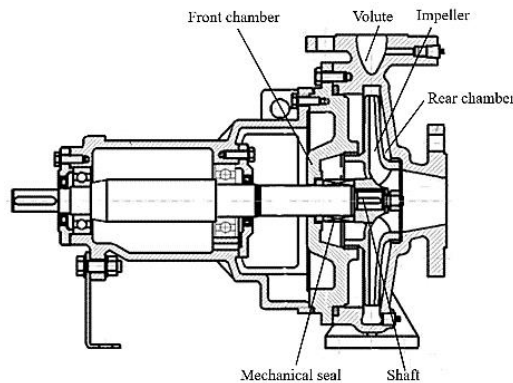


Fig. 1. Schematic of fire pump structure.

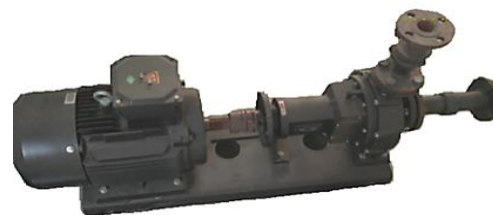


Fig. 2. Physical object of the fire pump.

2.2 Experimental Analysis of Fire Pump Performances

Figure 3 shows the experimental performance curves of the fire pump; the design head of the fire pump is 75.68 m. Comparing the two special flow rates of $0Q_d$ and $1.5Q_d$, it can be observed that the head of the fire pump is 74.02m at $0Q_d$, which is 1.66 m lower than $1.0Q_d$, and the head of the fire pump at $1.5Q_d$ is 74.82m which is 0.86m lower than $1.0Q_d$. Therefore, it can be found that the head curve of the fire pump has a hump.

The efficiency curve of the fire pump shows a continuous upward trend, but its highest efficiency point does not appear at $1.0Q_d$. Simultaneously, the efficiency of the fire pump at $1.0Q_d$ was 36.84%, failing to meet the design requirements of 38%.

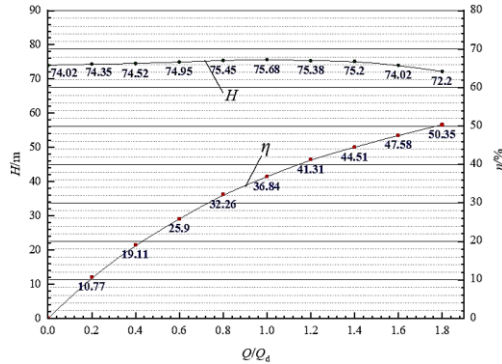


Fig. 3. Experimental performance curves of fire pump.

3. HYDRAULIC OPTIMIZATION

3.1 Numerical Calculation Method

First, a full flow-field numerical calculation was performed for the fire pump. The main calculation domain included the pump impeller, volute, and the front and back pump chambers. In addition to the main calculation domain, extensions of 10 times the pipe diameter were added to the impeller inlet and volute outlet to ensure the full development of fluid in the calculation domain. The above computational domain models were modeled using Pro/E 5.0. The main calculation domains are shown in Fig. 4.

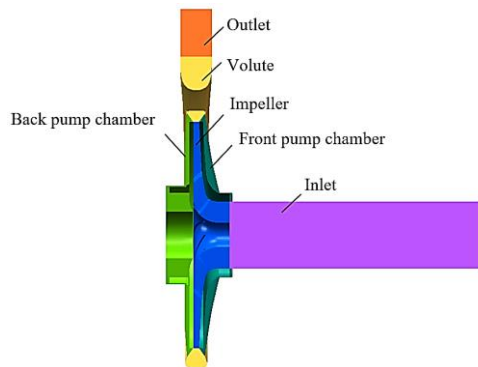


Fig. 4. Calculation of domain water body.

The grid is important for numerical calculations, and the division of the grid has a significant impact on the accuracy of the calculation results and the occupation of computing resources. To select the best meshing scheme, ICEM was used to divide the computational domain into hexahedral-structured meshes, and the number of meshes on the interface was maintained at the same magnitude. Six schemes

with different grid numbers were divided, and numerical calculations under the same conditions were performed for the six grid schemes. The grid division schemes and calculation results are presented in Table 1 and Fig. 5, respectively. As shown in Table 1 and Fig. 5 (Lei *et al.* 2018), the number of grids had a certain impact on the calculation results. With an increase in the number of grids, the predicted head value gradually decreased. When the number of grids increases to the number in scheme 5, the predicted head and efficiency change range remains within $\pm 0.1\%$. It can be considered that scheme 5 can eliminate the influence of the number of grids on the calculation results. Therefore, scheme 5 was selected for the follow-up numerical calculation, and its grids are shown in Fig. 6. The y^+ (Fu *et al.* 2015) value of the entire computational domain was always lower than 100, and the maximum y^+ value of the impeller computational domain was 54.91.

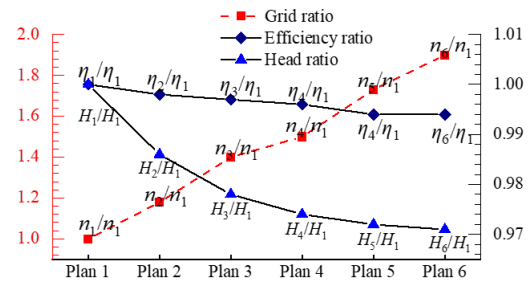


Fig. 5. Verification of grid independence of fire pump.

ANSYS CFX was used to numerically calculate the fire pump, and the calculation domain was divided into six parts: the inlet extension, impeller, volute, front pump chamber, back pump chamber, and outlet extension section.

The RNG $k-\epsilon$ turbulence model was employed for numerical calculations (Liu *et al.* 2013; Wang *et al.* 2016; Li *et al.* 2020). The calculation of the inlet refers to the total pressure inlet; the value of the total pressure is 1atm and the Intensity is 5%. The outlet was the mass flow rate outlet, the design mass flow rate was 3.47 kg/s; the shut-off condition (i.e. $0Q_d$) (Dyson and Teixeira. 2004) was usually taken to be the mass flow rate of the seal ring leakage, which is about 1%-5% of the pump design flow rate. Since the pump design flow rate was 3.47kg/s, the outlet mass flow rate was 0.035kg/s at $0Q_d$. The wall surface of each calculation domain was a non-slip wall, and the roughness of the front and back chambers was 3.2, that is, 32 μ m. The roughness of the blade surface and volute was 6.4, and the rest were set to 12.5. High resolution was adopted for the advection scheme and turbulence numerics. The total time of the unsteady calculation was 0.20339s, and the calculation step was 1.12994×10^{-4} s, that is, the impeller was solved once for every 2° rotation of the flow field; for a total of 10 rotational cycles. Additionally, Zwart–Gerber–Belamri (ZGB) model (Zwart *et al.* 2004) was applied to investigate the cavitation (two-phase) flow inside the pump. Cavitation in the pump is achieved by reducing the pressure at the pump inlet.

Table 1. Verification of grid independence of fire pump

Scheme	Grid number ($\times 10^4$)	H (m)	η (%)	H/H_1	η/η_1
Scheme 1	180.27	79.04	37.41	1	1
Scheme 2	213.03	77.96	37.32	0.986	0.998
Scheme 3	252.31	77.31	37.29	0.978	0.997
Scheme 4	274.98	77.06	37.27	0.974	0.996
Scheme 5	312.22	76.84	37.21	0.972	0.994
Scheme 6	342.73	76.79	37.21	0.971	0.994

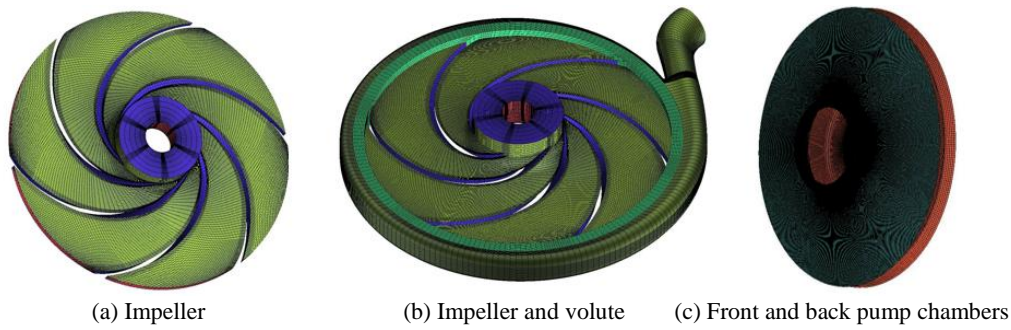


Fig. 6. Grid of the fire pump.

3.2 Numerical Calculation and Experimental Verification

Figure 7 shows the performance curves of the fire pump obtained using experiments and numerical calculations. From the figure, that the external characteristic curve of the fire pump obtained by numerical calculation is consistent with the experiment, where the experiment head of the fire pump at $1.0Q_d$ is 75.68m, the numerical calculation head of the fire pump at $1.0Q_d$ is 76.38m, and the error between the numerical calculation and the experiment value is within 1%. Simultaneously, it can be observed from the external characteristic curve that the head curves obtained in both methods show a hump, which needs to be further optimized.

3.3 Design Scheme

The fire pump prototype was designed using an increased flow rate design approach. This design method increases the impeller outlet b_2 and blade outlet angle β_2 to obtain a flat head curve and high efficiency. Simultaneously, the actual operation of the fire pump is at a low flow rate owing to the design method, which directly leads to a high impact loss inside the fire pump and hump of the head curve.

First, the hump phenomenon of the fire pump is optimized. The blade outlet width b_2 was reduced from 7mm to 5.5mm, and the blade outlet angle β_2 was reduced from 40° to 32° (Han *et al.* 2018; Wang

et al. 2019). However, the reduction of b_2 and β_2 will reduce the design head of the fire pump; therefore, an optimization method for the long and short blade composite impellers and increasing the blade thickness was adopted, which can improve the design head, increase the impeller outlet constraint and reduce the discharge coefficient of the impeller inlet. To further eliminate the separation flow in the impeller and improve the efficiency, an increase in the blade wrap angle and inclination of the blade outlet edge was adopted to reduce the pressure pulsations of the pump. The impeller parameters of the optimization scheme are listed in Table 2, and the three-dimensional impeller of the optimized scheme is shown in Fig. 8.

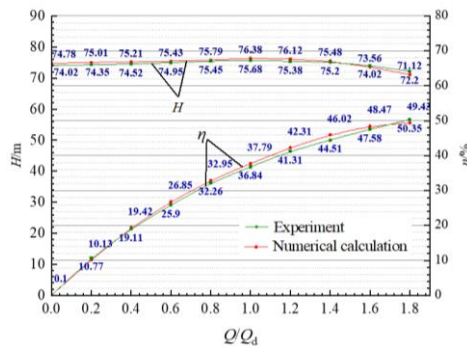


Fig. 7. Experimental and numerical calculation performance curves of the fire pump.

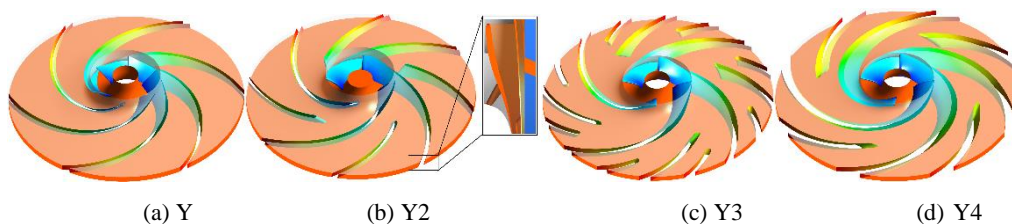


Fig. 8. Optimized impeller schemes in three-dimensional.

Table 2. Fire pump impeller optimized scheme

Impeller scheme	Blade outlet width	Blade outlet angle	Number of blades	Blade thickness		Blade wrap angle	Blade outlet mode
				Blade hub	Blade rim		
Y	7mm	40°	6	2.6mm	4mm	150°	Vertical
Y2	5.5 mm	32°	4 long blades and 4 short blades	4mm	5.4mm	135°	Inclined
Y3	5.5 mm	32°	4 long blades, 4 medium length blades, and 8 short blades	4mm	5.4mm	135°	Inclined
Y4	5.5 mm	32°	4 long blades and 4 short blades	4mm	6mm	200°	Inclined

4. OPTIMIZATION ANALYSIS AND EXPERIMENTAL VERIFICATION

4.1 Comparative Analysis of Optimization Scheme Performance

Figure 9 illustrates the performance curves of the original scheme and three optimized schemes. It can be observed from Fig. 9 that the changing trend of the head curve of the four schemes is slightly different. The head of the Y3 scheme at each flow rate is higher than that of the other schemes, but there is a hump in the head curve. The head curve of the Y2 scheme is flatter, and the head of the Y4 scheme gradually decreases with an increase in the flow rate.

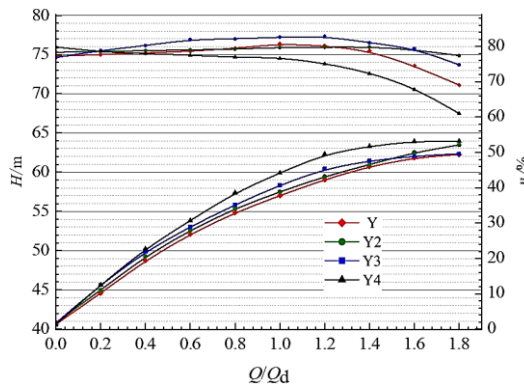


Fig. 9. Comparison of performance curves between the original scheme and the optimized schemes.

Comparing the efficiency of the schemes at $1.0Q_d$, it can be concluded that the changing trend of the efficiency of each scheme is also different with the increase in flow rate. The upward trend of the efficiency of the Y2 scheme is the most obvious, followed by the Y scheme, but the best efficiency point of both schemes exceeds $1.8Q_d$. In contrast, the efficiency of the Y3 and Y4 schemes increases with an increase in the flow rate, which gradually slows down after $1.2Q_d$ and reaches the highest point at $1.8Q_d$. The efficiencies of each scheme at $1.0Q_d$ were 37.79%, 38.85%, 40.72%, and 41.03%, respectively.

Comprehensive analysis shows that the head curve of the Y4 scheme avoids the hump and meets the requirements of the fire pump. Moreover, the efficiency of the Y4 scheme at the design flow rate was 4.2% higher than that of the original scheme, which was the best of all schemes.

4.2 Comparative Analysis of Internal Flow Characteristics

To investigate the differences between the original scheme and the optimized scheme of the fire pump impeller, the streamline distribution on the cross-section of the impeller channel with different blade heights at $0Q_d$, $1.0Q_d$, and $1.5Q_d$, were selected for comparative analysis.

Figure 10 shows the streamline distributions colored according to the velocity magnitude of each scheme with different blade heights under the shut-off condition. It can be observed from the figure that, in the Y and Y2 schemes, the outlet of all flow channels of the impeller is filled with large-scale vortices, and the vortex scale is similar at the height of 0.1 span to 0.9 span. In contrast, the vortex scale in the flow channels Y3 and Y4 was relatively small, and some of the flow channels maintained a relatively good flow capacity. Simultaneously, the vortex scales of the Y3 and Y4 schemes at 0.5span and 0.9span are smaller than that of span of 0.1, indicating that the Y3 and Y4 schemes reduce the axial size of the stall zone to a certain extent and reduce the impact of the flow disturbance at $0Q_d$.

As shown in Fig. 11, the streamline distributions are colored by the velocity magnitude on the cross-section of the impeller channel with different blade heights at $1.0Q_d$ respectively. As can be observed from Fig. 11, at a height of 0.1span, there is a distribution of stall vortices in the flow channels of all the schemes. The Y and Y2 schemes also have larger-scale vortices at the blade outlets, whereas the Y3 and Y4 schemes have more obvious separation flows on the pressure side of the blades. Comparing the streamline distribution of the 0.5span and 0.9span schemes, it can be observed that Y4 scheme has a smaller impulse angle between the inlet flow and the blades, and the flow state is better. The vortex flow in the Y and Y2 flow channels developed at the inlet edge of the blade, which had a negative impact on the inlet flow (Chen *et al.* 2022a,b; Lin *et al.* 2021).

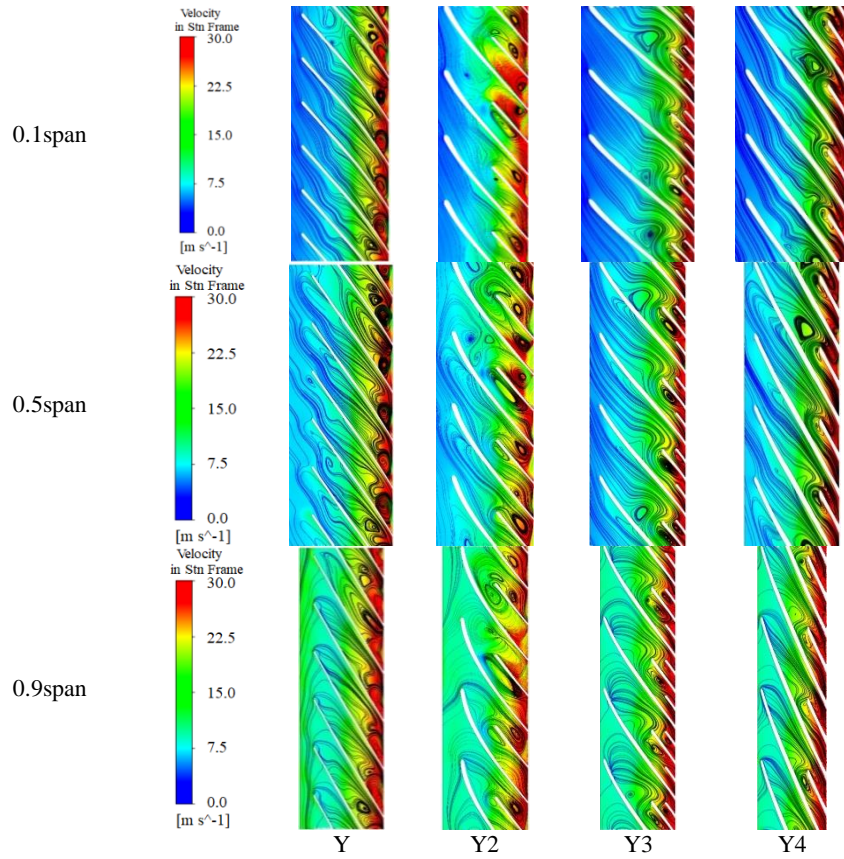


Fig. 10. Streamline distributions colored by the velocity magnitude on the cross-section of the impeller channel with different blade heights at $0Q_a$.

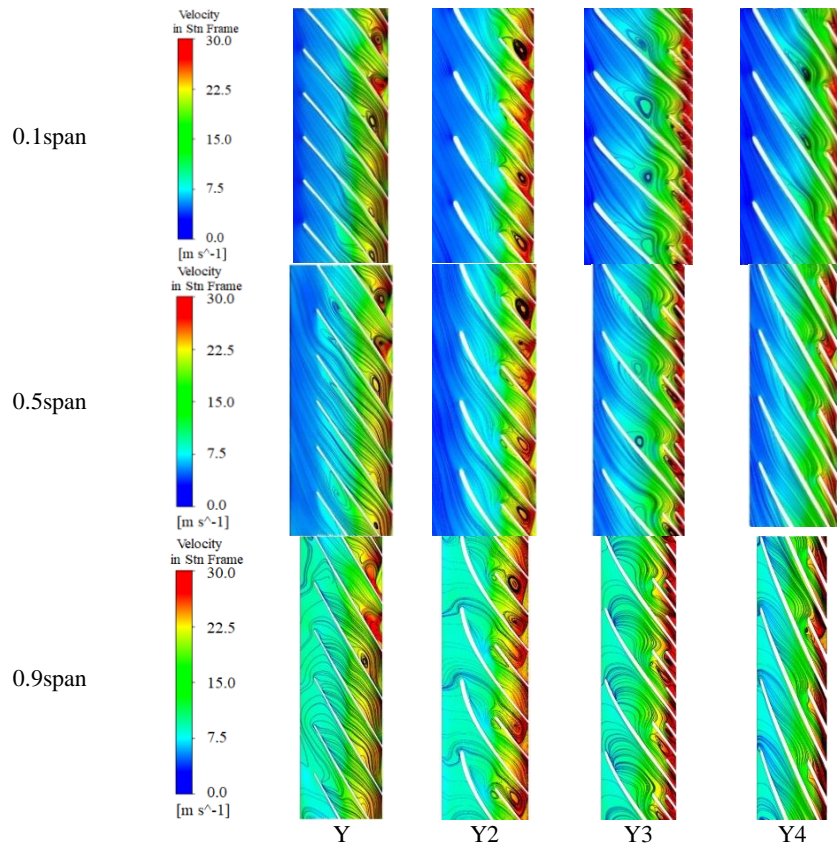


Fig. 11. Streamline distributions colored by the velocity magnitude on the cross-section of the impeller channel with different blade heights at $1.0Q_a$.

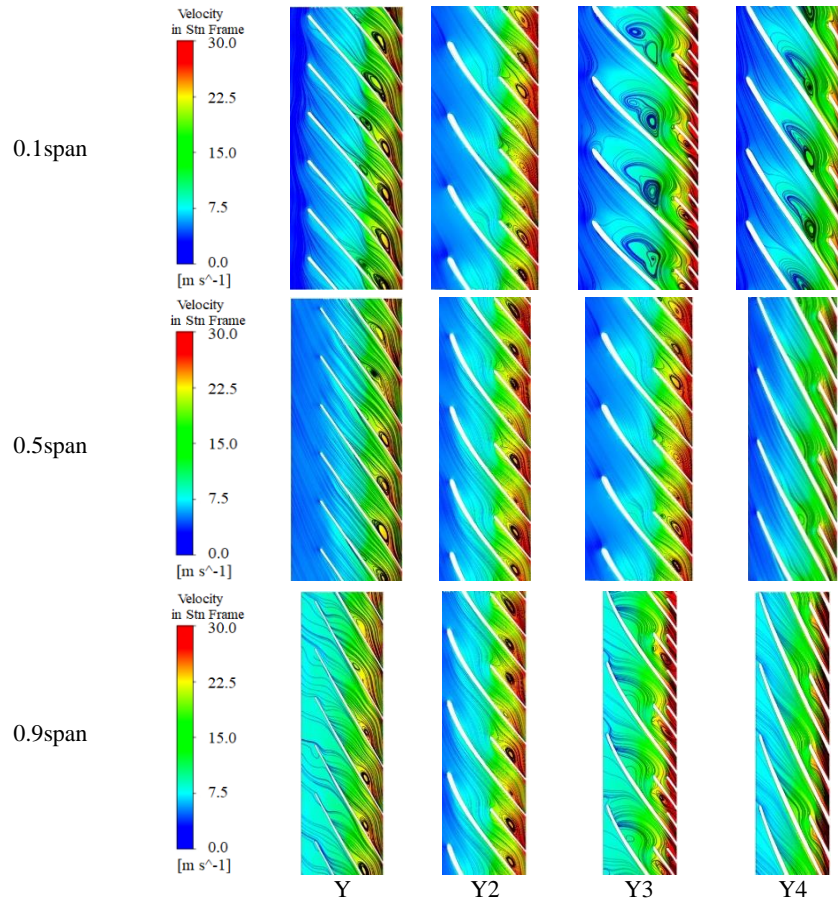


Fig. 12. Streamline distributions colored by the velocity magnitude on the cross-section of the impeller channel with different blade heights at $1.5Q_d$

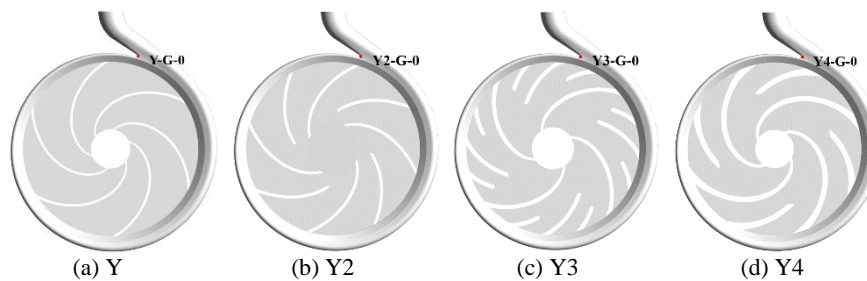


Fig. 13. Pressure pulsations monitoring point of each scheme.

The streamline distribution on the cross-section of the impeller channel with different blade heights at $1.5Q_d$ can be observed in Fig. 12. The vortex generated by the flow separation in the Y, Y2, and Y3 schemes runs through the entire impeller channel at a high flow rate, and there is a significant relative velocity slip at the outlet of the flow channels in the Y and Y2 schemes. In contrast, the vortex in the Y4 scheme is significantly reduced at 0.5 span, the streamline distribution tends to be uniform, the inlet streamline remains parallel to the blade, and there is no obvious slip phenomenon at the outlet channel.

4.3 Comparative Analysis of Pressure pulsations

Figure 13 shows the locations of the monitoring points of the pressure pulsations in the volute tongue. To compare the pressure pulsations of the fire pump

at different flow rates more intuitively, the pressure pulsations coefficient C_p was introduced to measure the magnitude of the pressure pulsations as follows:

$$C_p = 2(P - \bar{P}) / \rho u^2 \quad (1)$$

where P is the static pressure at a certain time, \bar{P} is the average static pressure, u is the circumferential speed of the impeller outlet, and ρ is the density of the water.

First, the pressure pulsations at the volute tongue of each scheme were dimensionless, and the results are observed in Fig. 14. It can be seen from the time domain results of pressure pulsations at the volute tongue position of each scheme in Fig. 14 that the peaks and valleys of the pressure pulsation time-domain characteristics are the same as the number of

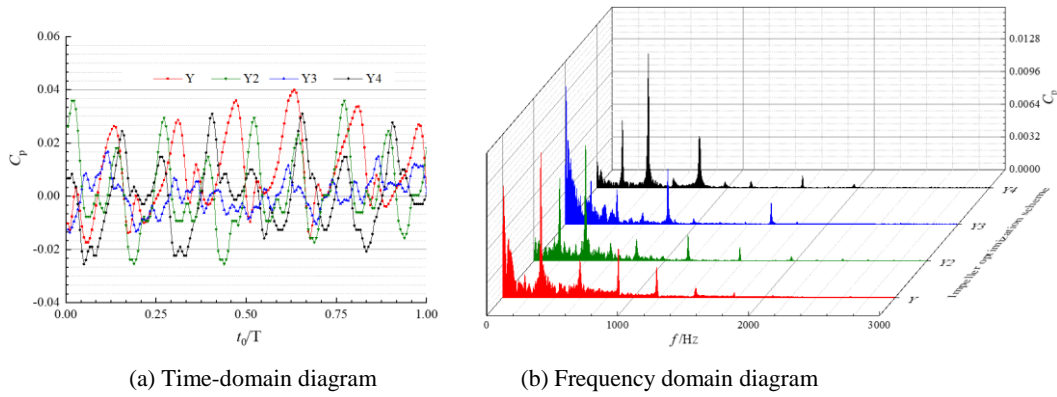


Fig. 14. Pressure pulsations at the volute tongue of each scheme at $0Q_d$.

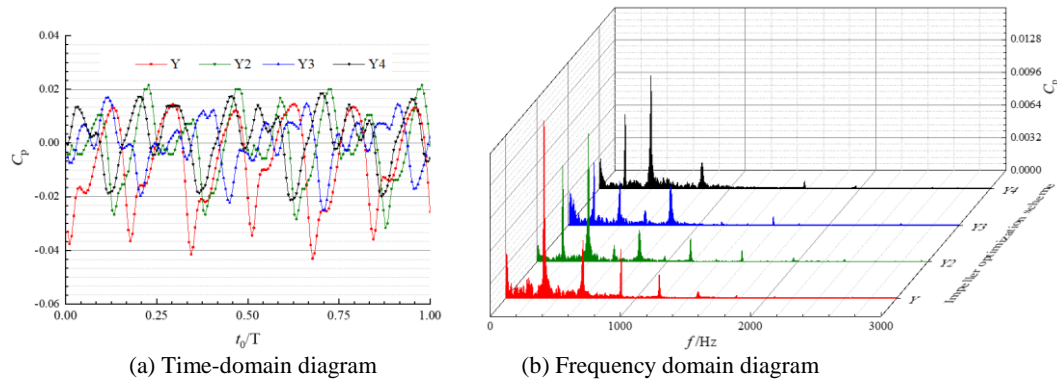


Fig. 15. Pressure pulsations at the volute tongue of each scheme at $1.0Q_d$.

blades under the shut-off condition. This proved that the pressure pulsations at the volute tongue of each scheme are caused by the rotor-stator interaction of the fire pump. Comparing the amplitude of the pressure pulsations coefficients of each scheme, it can be observed that the difference in the amplitude of the pressure pulsation coefficients of the Y, Y2, and Y4 schemes is not significant, while that of the Y3 scheme is lower than that of the other three schemes. It can be concluded that an increase in the number of blades has a strong suppression effect on the pressure pulsations at the volute tongue at $0Q_d$. Comparing the pressure pulsations frequency domain diagrams, it can be observed that the frequency domain distribution of the pressure pulsation coefficients at $0Q_d$ for each scheme is dominated by the blade passing frequency (BPF) and is accompanied by the harmonic frequency of the blade passing frequency (nBPF). In addition, both the Y and Y3 schemes have many small peaks in the low-frequency section, which may be related to the vortex caused by the separated flow at the volute tongue.

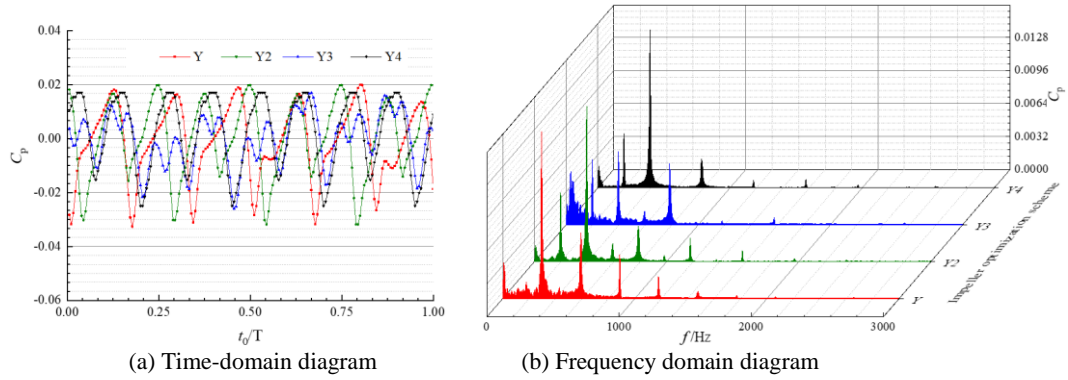
Figure 15 shows that the pressure pulsations coefficient at the volute tongue of the optimized schemes reduces, and the order of the pressure pulsations coefficient at the volute tongue of each scheme is $Y4 < Y3 < Y2 < Y$. Comparing the frequency domain distribution of the pressure pulsations coefficients of each scheme, it can be observed that at the design flow rates, the main frequencies of each scheme are still BPF and nBPF.

Compared to the $0Q_d$, there is no significant change in the amplitude of the pressure pulsations at the characteristic frequencies of the Y2 and Y4 schemes, while the peak of the low-frequency section of the Y scheme and the Y3 scheme decreased significantly at the design flow rate, indicating that the separation flow at the volute tongue of the Y scheme and the Y3 scheme at the design flow rate had been improved.

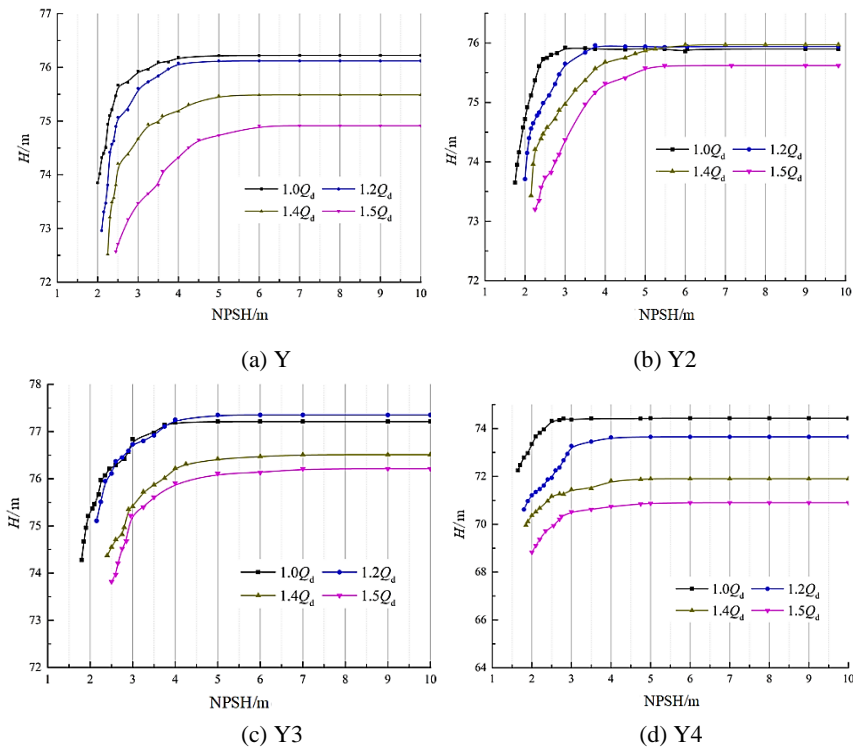
As shown in Fig. 16, when the flow rate increases to $1.5Q_d$, the amplitude of the pressure pulsation coefficient of scheme Y decreases significantly, while the optimized scheme remains unchanged. However, the pulsation coefficient of scheme Y is still greater than that of the optimized schemes. At $1.5Q_d$, the order of the pressure pulsation coefficient amplitude for each scheme is $Y3 < Y4 < Y2 = Y$. In terms of the frequency domain distribution, except that the peak value of the pressure pulsation coefficient in the low-frequency section of the Y3 scheme has increased, the peak value of the pressure pulsation coefficient in the other schemes has little change compared with the design flow rate.

4.4 Cavitation Characteristic Analysis

Through the numerical calculation of the cavitation performance of each scheme, the results of the cavitation performance of each scheme are shown in Fig. 17 and Table 3. Net positive suction head (Ali and Javed 2020) (*NPSH*) is the difference between the total pressure head at the inlet and the vapor pressure head of the fluid. Critical net positive suction head



(a) Time-domain diagram (b) Frequency domain diagram
Fig. 16. Pressure pulsations at the volute tongue of each scheme at $1.5Q_d$.



(a) Y (b) Y2 (c) Y3 (d) Y4
Fig. 17. Cavitation performance curves of the fire pump.

($NPSH_r$) (Pei *et al.* 2019) is accepted as a criterion, and the value of $NPSH_r$ was defined as the $NPSH$ corresponding to a 3% drop in head under cavitation compared to no cavitation.

$$NPSH = \frac{P_{in}}{\rho g} + \frac{v_{in}^2}{2g} - \frac{P_v}{\rho g} \quad (2)$$

where P_{in} and v_{in} are the absolute pressure and velocity at the pump inlet, respectively, and P_v is the vapor pressure ($P_v=3574$ Pa at 25°C) of water.

It can be observed from Fig. 17 that the changing trend of the head with $NPSH$ in each scheme is consistent. At the design flow rate, the head curve of each scheme remained unchanged when $NPSH$ began to decrease. When the $NPSH$ is reduced to 4 m, the Y and Y3 schemes are the first to start decreasing, and the head curves of the Y2 and Y4 schemes begin to decline when $NPSH$ is 3 m. The heads of the four schemes decreased by 3% when

$NPSH_r$ was reduced to 2 m, 1.75 m, 1.8m, and 1.65 m, respectively. At $1.2Q_d$, the $NPSH_r$ of each scheme is 2.10 m, 2.0 m, 2.15 m, and 1.8 m respectively; at $1.4Q_d$, it is 2.25 m, 2.15 m, 2.4 m, and 1.85 m, and at $1.5Q_d$, it is 2.45 m, 2.25 m, 2.5 m and 2.0 m. It can be observed that the $NPSH_r$ of the Y4 scheme at each flow rate is reduced by 17.5%, 14.2%, 17.7%, and 18.3% compared to the original scheme, which is the best cavitation performance scheme.

Table 3. Comparison of $NPSH_r$ of various schemes

Scheme	$1.0Q_d$	$1.2Q_d$	$1.4Q_d$	$1.5Q_d$
Y	2.0m	2.10m	2.25m	2.45m
Y2	1.75m	2.0m	2.15m	2.25m
Y3	1.80m	2.15m	2.4m	2.5m
Y4	1.65m	1.8m	1.85m	2.0m

5. EXPERIMENTAL VERIFICATION

The external characteristics, pressure pulsations characteristics, and cavitation performance of the original scheme and three optimized schemes were analyzed. According to the numerical calculation and analysis results, it can be observed that the Y4 scheme has no hump in the head curve, and the efficiency at the design flow rate is improved by 9.17% compared to the original scheme, therefore, the Y4 scheme is selected as the best-optimized scheme for experimental verification. Figure 18 shows the three-dimensional model and the physical object of the optimized Y4 impeller.

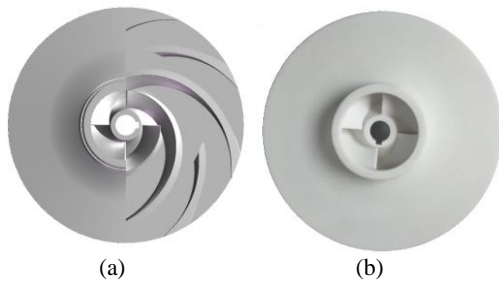


Fig. 18. Optimized scheme Y4 impeller: (a) Three-dimensional model of the impeller (b)Physical object of the impeller.

5.1 Comparative Analysis of Performance Experiments

A performance curve comparison between the optimized and original schemes is shown in Fig. 19. As can be observed from the figure, the experimental head of the original scheme at the $1.0Q_d$ is 75.68m, and the optimized scheme is 74.43m, and both schemes can meet head requirements while the optimized scheme is closer to the design requirements at the design flow rate. The experimental heads of the optimized scheme at $0Q_d$ and $1.5Q_d$ are 77.21 m and 70.14 m respectively, which are $1.02H_d$ and $0.93H_d$ respectively, compared with the head at $1.0Q_d$. The optimized scheme not only meets the design requirements of the fire pump but also eliminates the hump phenomenon.

Comparing the efficiency curves of the original and optimized schemes, it can be observed that the efficiency curve of the optimized scheme is higher than that of the original scheme. At $1.0Q_d$, the experimental efficiency of the optimized scheme was 40.22%, which was 3.38% higher than that of the original scheme, and the efficiency of the fire pump was significantly improved.

Comparing the power curves of the original and optimized schemes, it can be observed that the power curve of the optimized scheme is lower than that of the original scheme, and the power of the fire pump is optimized.

5.2 Comparative Analysis of Pressure Pulsations Experiments

Owing to the difference between the heads of the original scheme and the optimized scheme, the pressure pulsation is first subjected to dimensionless

processing to obtain the frequency domain of the inlet and outlet pressure pulsation coefficients, as shown in Fig. 20. It can be observed from the figure that the main frequency of the pressure pulsations at the outlet of the original and optimized schemes is 1 axial pass frequency (APF), and the second frequency is 1BPF at $0Q_d$. The peak value of the pressure pulsation coefficient at 1BPF of the original scheme was 0.008, and the peak value of the optimized scheme was 0.006, which was 25% lower than that of the original scheme. Simultaneously, only the 2BPF and 3BPF are the more obvious harmonic frequencies in the optimized scheme, and the number of harmonic frequencies is reduced compared to the original scheme.

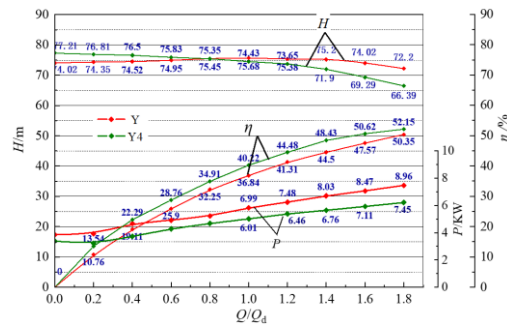


Fig. 19. Performance curve comparison between the optimized scheme and the original scheme.

Comparing $1.0Q_d$ and $1.5Q_d$, it can be observed that at $1.0Q_d$, the primary and secondary frequency distributions of the original scheme maintain the same trend at $0Q_d$. In contrast, the primary frequency of the optimized scheme appears at 1BPF, accompanied by the harmonic frequencies of the 2 BPF and 3 BPF. As the flow rate increases to $1.5Q_d$, the primary frequency of the original scheme and the optimized scheme is 1 APF and the second frequency is 1 BPF. Simultaneously, the peak value of the pressure pulsations coefficient at 1BPF was 0.0068 in the original scheme and 0.0042 in the optimized scheme, which is a reduction of 38.2% compared to the original scheme. It can be concluded that the optimized scheme significantly reduces the influence of the rotor-stator interaction of the fire pump between the impeller and volute tongue, and ensures the stability of the outlet pressure.

5.3 Comparative Analysis of Cavitation Characteristics Experiments

Figure 21 shows the $NPSH$ of the optimized and original schemes from $1.0Q_d$ to $1.5Q_d$. It can be observed from the comparison that the changing trend of the head with $NPSH$ for the optimized scheme is consistent with that of the original scheme. Comparing the $NPSH$ of the two schemes, at the design flow rate, the $NPSH_r$ of the original scheme and the optimized scheme was 1.95 m and 1.53 m, with a reduction of 21.5% compared with the original scheme. At $1.2Q_d$, $NPSH_r$ was 2.04m and 1.68m respectively, with a reduction of 17.6%. At $1.4Q_d$, $NPSH_r$ is 2.16m and 1.82m, a reduction of 15.7%. At $1.5Q_d$, $NPSH_r$ is 2.38m and 1.98m, with a decrease of 16.8%.

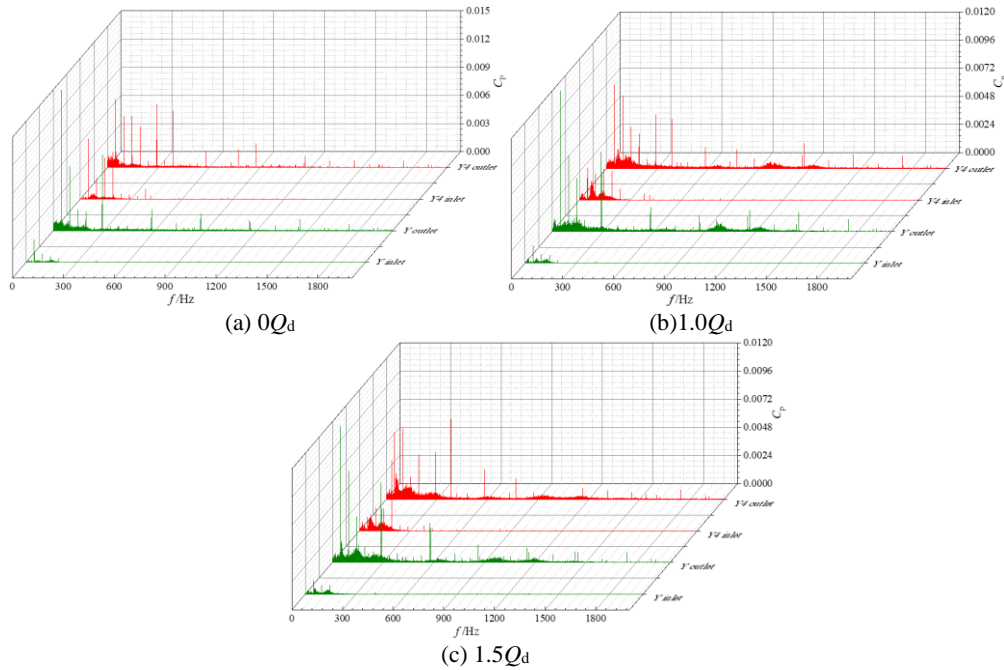


Fig. 20. Frequency domain distribution of inlet and outlet pressure pulsations coefficients of the optimized scheme and original scheme

Table 4. Comparison of $NPSH_r$ at different flow rates between optimized scheme and original scheme

Flow rate	$1.0Q_d$	$1.2Q_d$	$1.4Q_d$	$1.5Q_d$
Original scheme	1.95m	2.04m	2.16m	2.38m
Optimized scheme	1.53m	1.68m	1.82m	1.98m
$NPSH_r$ reduction ratio	21.53%	17.64%	15.74%	16.81%

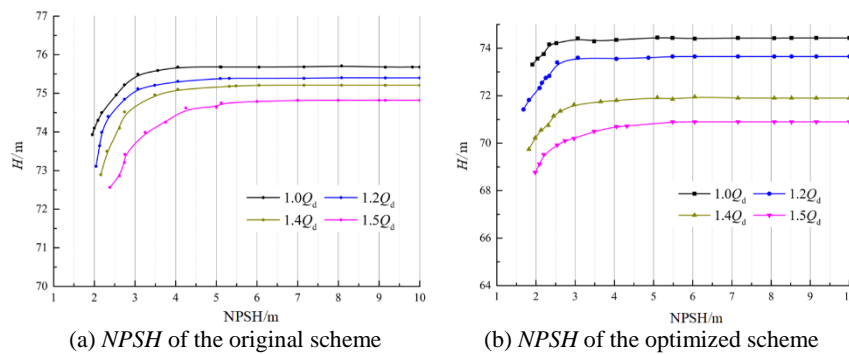


Fig. 21. Comparison of $NPSH$ between optimized scheme and original scheme.

A comparison of $NPSH_r$ at each flow rate is shown in Table 4. It can be observed from the table, that the cavitation performance of the optimized scheme at the four flow rates was more than 15% higher than that of the original scheme. Therefore, the optimized scheme successfully optimizes the cavitation performance of the fire pump and guaranteed its safe operation of the fire pump.

6. CONCLUSIONS

By comparing the problems of a centrifugal fire pump with a speed of 24.7, optimized schemes were proposed, analyzed by numerical simulation, and verified experimentally. The main conclusions are as follows.

(1) Because the prototype fire pump adopts the design method of increasing the flow rate, the hump phenomenon occurs at low flow rates.

(2) By reducing the blade outlet width b_2 and blade outlet angle β_2 , increasing the blade wrap angle, adopting a composite impeller with long and short blades, blade outlet side inclination, and increasing the blade thickness design method, the Y1, Y2, Y3, and Y4 schemes were obtained. Numerical calculations were used to compare and analyze the performance of the fire pump before and after optimization. The results show that the efficiency of the Y4 scheme at the design flow rate increased by 9.17% compared with the original scheme, and the head met the fire pump design requirements while

avoiding the occurrence of the hump phenomenon. Through a comparative analysis, it was found that the optimized scheme Y4 can reduce the pressure pulsations at the pump outlet and optimize the cavitation performance at different flow rates. Compared with the original scheme, the $NPSH_r$ at $1.0Q_d$, $1.2Q_d$, $1.4Q_d$, and $1.5Q_d$ were reduced by 17.5%, 14.2%, 17.7%, and 18.3%, respectively, compared with the original scheme.

(3) The optimized scheme Y4 was experimentally investigated and verified, and the results show that the head of the optimized fire pump is 74.43m, the efficiency is 40.22% at the design flow rate, and the head curve is without a hump, which meets the design and uses requirements of the fire pump. The optimized scheme reduced the pressure pulsations of the pump outlet, with an average reduction of 47.12% in the maximum drop in the outlet pressure pulsation coefficient at $0Q_d$, $1.0Q_d$, and $1.5Q_d$. The $NPSH_r$ of the fire pump at $1.0Q_d$, $1.2Q_d$, $1.4Q_d$, and $1.5Q_d$ are 1.53 m, 1.68 m, 1.82 m, and 1.98 m respectively, which are reduced by 21.5%, 17.6%, 15.7%, and 16.8% respectively compared with the original scheme, and the cavitation performance of the optimized scheme has been improved.

ACKNOWLEDGEMENTS

This work was supported by the National Natural Science Foundation of China (Grant No. 52179084), and China Postdoctoral Science Foundation (Grant No. 2021M692709).

REFERENCES

- Adu, D., J. Du, R. O. Darko, E. O. Antwi and M. Khan (2021). Numerical and experimental characterization of splitter blade impact on pump as turbine performance. *Science progress* 104(2),1-15.
- Ali, M. and A. Javed (2020). Numerical Analysis of Flow Phenomena in a Centrifugal Pump Impeller of Low Specific Speed. *2020 17th International Bhurban Conference on Applied Sciences and Technology (IBCAST)*.
- Chabannes, L., D. Tefan and P. Rudolf (2021). Effect of splitter blades on performances of a very low specific speed pump. *Energies* 14(13), 3785.
- Chen, B., X Li and Z Zhu (2022a). Investigations of energy distribution and loss characterization in a centrifugal impeller through PIV experiment. *Ocean Engineering* 247, 110773.
- Chen, B., X Li and Z Zhu (2022b). Time-Resolved Particle Image Velocimetry Measurements and Proper Orthogonal Decomposition Analysis of Unsteady Flow in a Centrifugal Impeller Passage. *Frontiers in Energy Research* 9, 818232.
- Dyson, G. and J. Teixeira (2009). Investigation of closed valve operation using computational fluid dynamics. *Proceedings of the ASME 2009 Fluids Engineering Division Summer Meeting*.
- Fu, Y. X., J. P. Yuan, S. Q. Yuan, G. Pace, L. d'Agostino, P. Huang and X. J. Li (2015). Numerical and experimental analysis of flow phenomena in a centrifugal pump operating under low flow rates. *Journal of Fluids Engineering* 137(1), 011102.
- Han, X., Y. Kang, D. Li and W. Zhao (2018). Impeller optimized design of the centrifugal pump: A numerical and experimental investigation. *Energies* 11(6), 1444.
- Kocaaslan, O., M. Ozgoren, M. H. Aksoy and O. Babayigit (2016). Experimental and numerical investigation of coating effect on pump impeller and volute. *Journal of Applied Fluid Mechanics* 9(5), 2475-2487.
- Lei, T., Z. Xie, Y. Liu, H. Yue and X. Yun (2018). Influence of t-shape tip clearance on performance of a mixed-flow pump. *Proceedings of the Institution of Mechanical Engineers Part A Journal of Power and Energy* 232(4), 386-396.
- Li, X., T. Shen, P. Li, X. Guo and Z. Zhu (2020). Extended compressible thermal cavitation model for the numerical simulation of cryogenic cavitating flow. *International Journal of Hydrogen Energy* 45(16), 10104-10118.
- Lin, Y., X. Li, B. Li and X. Jia (2021). Influence of impeller sinusoidal tubercle trailing edge on pressure pulsation in a centrifugal pump at nominal flow rate. *ASME Journal of Fluids Engineering* 143 (9) 091205.
- Liu, H. L., D. X. Liu, Y. Wang, X. F. Wu, J. Wang and H. Du (2013). Experimental investigation and numerical analysis of unsteady attached sheet-cavitating flows in a centrifugal pump. *Journal of Hydrodynamics* 25(3), 370-378.
- Menin, J. A. and E. Iguama (2006). Hydraulic drive improves fire pump availability. *World Pumps* (480), 38-39.
- Namazizadeh, M., M. T. Gevari, M. Mojaddam and M. Vajdi (2020). Optimization of the splitter blade configuration and geometry of a centrifugal pump impeller using design of experiment. *Journal of Applied Fluid Mechanics* 13(1), 89-101.
- Paluch, M. and M. Noga (2020). Design of an impeller for a fire fighting pump. *Journal of Physics: Conference Series* 1619(1), 012009.
- Pei, J., M. K. Osman, W. Wang, J. Yuan and D. Appiah (2019). Unsteady flow characteristics and cavitation prediction in the double-suction centrifugal pump using a novel approach. *Proceedings of the Institution of Mechanical Engineers Part A Journal of Power and Energy* 234(3), 095765091986363.
- Rosa, H. and B. S. Emerick (2020). CFD simulation on centrifugal pump impeller with splitter blades. *Revista Brasileira de Engenharia Agrícola e Ambiental* 24(1), 3-7.

- Shi, W. D., D. S. Zhang, W. G. Lu and W. D. Cao (2009). Design and experimental study on low-specific centrifugal fire pumps. *China Mechanical Engineering* 20(5), 514-517.
- Vasiljeva, O., I. Pasnak and A. Renkas (2020). Devising a method for ensuring the reliability of fire centrifugal pumps while reducing their weight and dimension characteristics by optimizing their structural elements. *Eastern-European Journal of Enterprise Technologies* 108(1), 14-19.
- Wang, K., G. Luo, Y. Li, R. Xia and H. Liu (2019). Multi-condition optimization and experimental verification of impeller for a marine centrifugal pump. *International Journal of Naval Architecture and Ocean Engineering* 12(1) 71-84.
- Wang, Y., H. Liu, D. Liu, S. Yuan, J. Wang and L. Jiang (2016). Application of the two-phase three-component computational model to predict cavitating flow in a centrifugal pump and its validation. *Computers & Fluids* 131, 142-150.
- Xu, Y., L. Tan, S. L. Cao and W. S. Qu (2016). Multiparameter and multiobjective optimization design of centrifugal pump based on orthogonal method. *ARCHIVE Proceedings of the Institution of Mechanical Engineers Part C Journal of Mechanical Engineering Science* 231(14), 2569-2579.
- Yang, X. X., W. W. Song, L. C. Wei, J. W. Shi and X. Wang (2017). Design and analysis of high-speed fire pumps. *Journal of Drainage & Irrigation Machinery Engineering* 35(12), 1036-1041.
- Yuan, Y. and S. Q. Yuan (2017). Analyzing the effects of splitter blade on the performance characteristics for a high-speed centrifugal pump. *Advances in Mechanical Engineering* 9(12), 1687814017745251.
- Zhang, J. F., Z. J. Yang, L. Q. Lai, H. Q. Song and C. M. Jing (2021). Automatic optimization of vertical long-shaft fire pump overload based on Particle Swarm optimization algorithm. *IOP Conference Series: Materials Science and Engineering* 1081(1), 012017.
- Zhang, R. H., X. B. Chen and J. Q. Luo (2020). Knowledge mining of low specific speed centrifugal pump impeller based on Proper Orthogonal Decomposition method. *Journal of Thermal Science* 30(3), 840-848.
- Zwart, P. J., A. G. Gerber and T. Belamri (2004). A two-phase flow model for predicting cavitation dynamics. *In Fifth international conference on multiphase flow*, 152.